

JGR Space Physics

RESEARCH ARTICLE

10.1029/2019JA026539

Key Points:

- We confine reconnection X-line within a thin current sheet using much thicker current sheets at two ends, which prevent the X-line spreading
- The shortest possible X-line for fast reconnection is $O(10d_i)$, relevant to the magnetic flux transport by e- in the anticurrent direction
- This flux transport can explain the reversed dawn-dusk asymmetry at Mercury's magnetotail, which has a short global dawn-dusk extent

Correspondence to:

Y.-H. Liu,
Yi-Hsin.Liu@Dartmouth.edu

Citation:

Liu, Y.-H., Li, T. C., Hesse, M., Sun, W.-J., Liu, J., Burch, J., et al. (2019). Three-dimensional magnetic reconnection with a spatially confined X-line extent: Implications for dipolarizing flux bundles and the dawn-dusk asymmetry. *Journal of Geophysical Research: Space Physics*, 124, 2819–2830. <https://doi.org/10.1029/2019JA026539>

Received 23 JAN 2019

Accepted 2 APR 2019

Accepted article online 11 APR 2019

Published online 25 APR 2019

Three-Dimensional Magnetic Reconnection With a Spatially Confined X-Line Extent: Implications for Dipolarizing Flux Bundles and the Dawn-Dusk Asymmetry

Yi-Hsin Liu¹, T. C. Li¹, M. Hesse^{2,3}, W. J. Sun⁴, J. Liu⁵, J. Burch³, J. A. Slavin⁴, and K. Huang^{1,6}

¹Department of Physics and Astronomy, Dartmouth College, Hanover, NH, USA, ²Department of Physics and Technology, University of Bergen, Bergen, Norway, ³Southwest Research Institute, San Antonio, TX, USA, ⁴Climate and Space Sciences and Engineering, University of Michigan, Ann Arbor, MI, USA, ⁵Department of Earth and Space Science, University of California, Los Angeles, CA, USA, ⁶Department of Geophysics and Planetary Science, University of Science and Technology of China, Hefei, China

Abstract Using 3-D particle-in-cell simulations, we study magnetic reconnection with the X-line being spatially confined in the current direction. We include thick current layers to prevent reconnection at two ends of a thin current sheet that has a thickness on an ion inertial (d_i) scale. The reconnection rate and outflow speed drop significantly when the extent of the thin current sheet in the current direction is $\lesssim O(10d_i)$. When the thin current sheet extent is long enough, we find that it consists of two distinct regions; a suppressed reconnecting region (on the ion-drifting side) exists adjacent to the active region where reconnection proceeds normally as in a 2-D case with a typical fast rate value ≈ 0.1 . The extent of this suppression region is $\approx O(10d_i)$, and it suppresses reconnection when the thin current sheet extent is comparable or shorter. The time scale of current sheet thinning toward fast reconnection can be translated into the spatial scale of this suppression region, because electron drifts inside the ion diffusion region transport the reconnected magnetic flux, which drives outflows and furthers the current sheet thinning, away from this region. This is a consequence of the Hall effect in 3-D. While the existence of this suppression region may explain the shortest possible azimuthal extent of dipolarizing flux bundles at Earth, it may also explain the dawn-dusk asymmetry observed at the magnetotail of Mercury, which has a global dawn-dusk extent much shorter than that of Earth.

1. Introduction

Through changing the magnetic connectivity, magnetic reconnection converts magnetic energy into plasma kinetic and thermal energies. It plays a critical role in the energy release of geomagnetic substorms both at Earth (Angelopoulos et al., 2008; Baker et al., 1996) and other planets (Kronberg et al., 2005; Mitchell et al., 2005; Slavin et al., 2010; Southwood & Chané, 2016; Sun et al., 2015). During reconnection, the magnetic connectivity is altered at geometrically special points, which constitute a “reconnection X-line” in the current direction. In a two-dimensional (2-D) model, the extent of the reconnection X-line is, technically, *infinitely* long due to the translational invariance out of the reconnection plane. It is of great interest to understand the fundamental nature of a three-dimensional (3-D) reconnection in the opposite limit. Especially, it remains unclear how a spatial confinement in the current direction would affect reconnection and whether there is a minimal requirement for the spatial extent of the reconnection X-line. Spatially confined reconnection can be relevant to azimuthally localized dipolarizing flux bundles (DFBs) at Earth's magnetotail (Li et al., 2014; Liu et al., 2013) and Mercury's entire magnetotail that has a short dawn-dusk extent (Poh et al., 2017; Rong et al., 2018; Sun et al., 2016).

DFBs are magnetic flux tubes embedded in fast earthward flows called bursty bulk flows (BBFs), and the leading edge of each DFB has been termed a dipolarization front. Observations show that they are localized in the azimuthal (i.e., dawn-dusk) direction with a typical extent of $3R_E$ (Nagai et al., 2013; Nakamura et al., 2004; Li et al., 2014; Liu et al., 2013), and the shortest extent observed is $\approx 0.5R_E \approx 10d_i$ (Liu et al., 2015). Here R_E is the Earth's radius and d_i is the ion inertial length. These fast earthward flows are observed

during substorms and have been associated observationally with Pi2 pulsations and the substorm current wedge (e.g., Kepko et al., 2015, and references therein). A localized DFB could originate from (1) an initially long dawn-dusk extended DFB that breaks up into smaller pieces (through interchange/ballooning instability) during the intrusion into the inner tail (Birn et al., 2011, 2015; Lapenta & Bettarini, 2011; Pritchett et al., 2014; Sitnov et al., 2014) or (2) simply from an azimuthally localized reconnection X-line, where the *frozen-in* condition is violated (Pritchett, 2013; Pritchett & Lu, 2018; Shay et al., 2003) within a finite azimuthal extent. While both mechanisms are possible in nature, in this work we study scenario (2) using a simple setup. In addition, spatially confined reconnection also has a direct application to the magnetotails of other planets, such as Mercury, whose global dawn-dusk extent is as short as a few tens of d_i (Poh et al., 2017; Rong et al., 2018; Sun et al., 2016). Interestingly, observations by MESSENGER (Sun et al., 2016) indicate a higher occurrence rate of DFBs on the dawnside of Mercury's magnetotail, opposite to that observed at Earth's magnetotail (whose extent is a few hundreds of d_i). An explanation to this dawn-dusk asymmetry is desirable.

Previous attempts that model the effect of the dawn-dusk localization on reconnection and BBFs are briefly summarized here. Shay et al. (2003) used initial perturbation spatially localized in the current direction to induce reconnection in two-fluid simulations. The shortest reconnection X-line in their simulation is $\approx 10d_i$ long, but the X-line spreads in the current direction unless the initial uniform current sheet is thicker than $4d_i$. In a follow-up study, Meyer (2015) derived a model of the outflow speed reduction using Sweet-Parker type analysis in 3-D diffusion regions. Dorfman et al. (2014) studied the localized reconnection region experimentally in Magnetic Reconnection Experiment (MRX). More recently, Arnold et al. (2018) used a 2-D Riemann setup to study the outflow reduction and suggested that the ion momentum transfer from the ion-drifting direction to the outflow direction is critical. Pritchett and Lu (2018) used a localized driving to study reconnection onset in tail geometry.

To study the effect of the dawn-dusk localization on reconnection, we confine the reconnection region by embedding a thin reconnecting current sheet between much thicker sheets. This spatial confinement strongly limits the spread of the X-line (Li et al., 2019; Nakamura et al., 2012; Shay et al., 2003; Shepherd & Cassak, 2012). This machinery allows us to study the 3-D nature of reconnection as a function of the X-line extent in a controlled fashion. Our simulations demonstrate that reconnection is strongly suppressed if the thin current sheet extent is shorter than a critical length of $\approx O(10d_i)$. Through detailed examinations of thin reconnecting current sheets of extent $31d_i$ and $8.4d_i$, we link this critical confinement scale to the extent of a suppressed reconnecting region on the ion-drifting side of the X-line, which connects to an active reconnection region with a typical fast (normalized) rate ≈ 0.1 on the electron-drift side. This two-region structure develops because the reconnected magnetic flux, which drives outflows and furthers the current sheet thinning, is preferentially transported by electrons in the direction of the electron drift. We show that the time scale toward fast reconnection can be translated into the spatial scale of this suppression region. This shortest possible X-line extent of $\sim O(10d_i)$ for fast reconnection manifested here can be relevant to the narrowest BBFs/DFBs observed at Earth's magnetotail (Liu et al., 2015). In addition, since the dawn-dusk extent of the entire magnetotail of Mercury is similar to the case considered here, the preferential transport of the reconnected magnetic flux to the electron-drifting side (i.e., the dawnside) can explain the observed dawn-dusk asymmetry of the occurrence rate of DFBs (Sun et al., 2016, 2017). In the end, we incorporate the dawn-dusk asymmetry argument in Lu et al. (2016, 2018) and propose that the opposite dawn-dusk asymmetry observed at Mercury and Earth is primarily caused by the vastly different global dawn-dusk scale.

The structure of this paper is outlined in the following. Section 2 describes the simulation setup. Section 3 shows the scaling of reconnection as a function of the confinement length scale. Section 4 shows the details of a case with a long confinement scale. Section 5 shows the details of a case with a short confinement scale. In section 6, we pin down the underlying physics that determines the critical confinement scale for suppression; section 6.1 examines the 3-D generalized Ohm's law. Section 6.2 examines the flux transport and the asymmetric thinning. Section 7 summarizes our results and proposes our explanation of the dawn-dusk asymmetry in planetary magnetotails.

2. Simulation Setup

The initial condition consists of the magnetic field $\mathbf{B}(y, z) = B_0 \tanh[z/L(y)]\hat{\mathbf{x}}$ and the plasma density $n(y, z) = n_0 \text{sech}[z/L(y)] + n_b$. Here the sheet half thickness $L(y) = L_{\min} + (L_{\max} - L_{\min})[1 - f(y)]$ with the

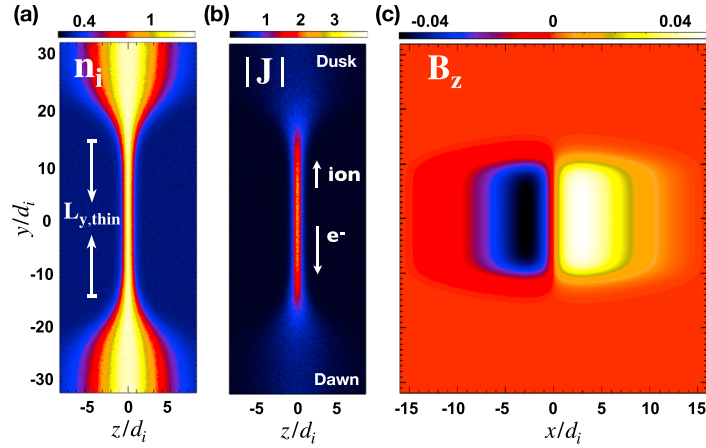


Figure 1. An example setup with $L_{y,\text{thin}} = 31d_i$. (a) The ion density n_i on the $x = 0$ plane. (b) The total current $|\mathbf{J}|$ on the $x = 0$ plane. (c) The initial magnetic perturbation B_z on the $z = 0$ plane.

function $f(y) = [\tanh((y + w_0)/S) - \tanh((y - w_0)/S)]/[2\tanh(w_0/S)]$. We choose $L_{\min} = 0.5d_i$, $L_{\max} = 4d_i$ and $S = 5d_i$ and the background density $n_b = 0.3n_0$, which will embed a thin sheet of thickness $1d_i (= 2 \times L_{\min})$ between the ambient thicker sheets of thickness $8d_i (= 2 \times L_{\max})$ in the y direction. In this work, we conduct runs with $w_0 = 20d_i, 10d_i, 7.5d_i$, and $2d_i$. We define the length of the thin current sheet $L_{y,\text{thin}}$ as the region for $L < 2 \times L_{\min} = 1d_i$, then the corresponding $L_{y,\text{thin}} = 31d_i, 12d_i, 8.4d_i$, and $4d_i$. We will use $L_{y,\text{thin}}$ to label the four runs discussed in this paper. For instance, the initial profiles of the $L_{y,\text{thin}} = 31d_i$ case is shown in Figure 1 for illustration. Figure 1a shows the density profile with $L_{y,\text{thin}}$ marked. Figure 1b shows the total current density $|\mathbf{J}|$. Note that ions (electrons) drift in the positive (negative) y direction that corresponds to the duskside (dawnside) at Earth's magnetotail. In addition to the y -varying current sheet thickness, we initiate reconnection with an initial perturbation within the thin current sheet region, as shown in Figure 1c. These four simulations have the domain size $L_x \times L_y \times L_z = 32d_i \times 64d_i \times 16d_i$ and $768 \times 1536 \times 384$ cells. The mass ratio is $m_i/m_e = 75$. Note that the growth of kinetic instabilities could be sensitive to the mass ratio. For instance, the drift-kink instability that prevails in many 3-D simulations can be suppressed with a more realistic (higher) mass ratio (Daughton, 1999). The simulations reported here appear to be kink stable. The ratio of the electron plasma to gyrofrequency is $\omega_{pe}/\Omega_{ce} = 4$ where $\omega_{pe} \equiv (4\pi n_0 e^2/m_e)^{1/2}$ and $\Omega_{ce} \equiv eB_0/m_e c$. In the presentation, densities, time, velocities, spatial scales, magnetic fields, and electric fields are normalized to n_0 , the ion gyrofrequency Ω_{ci} , the Alfvénic speed $V_A = B_0/(4\pi n_0 m_i)^{1/2}$, the ion inertia length $d_i = c/\omega_{pi}$, the reconnecting field B_0 , and $V_A B_0/c$, respectively. The boundary conditions are periodic both in the x and y directions, while in the z direction they are conducting for fields and reflecting for particles.

This setup will confine magnetic reconnection within the thin sheet region and prevent the reconnection X-line from progressively spreading into two ends (e.g., Li et al., 2019). Plasmas are loaded as drifting Maxwellians that satisfy the total pressure $P + B^2/8\pi = \text{const}$, and drifting speeds satisfy $\mathbf{J} = en(\mathbf{V}_{id} - \mathbf{V}_{ed}) = (c/4\pi)\nabla \times \mathbf{B}$ and $V_{id}/V_{ed} = T_i/T_e$ as in the standard Harris sheet equilibrium (Harris, 1962). These satisfy the relation $\mathbf{J} \times \mathbf{B} + \nabla P = 0$ and $\nabla \cdot \mathbf{B} = 0$. Note that the inertial force $m_i V_{iy} \partial_y V_{iy}$ in the transition regions (i.e., where $L(y)$ varies) does not vanish. To reduce this force that could move the entire structure in the $+y$ direction, we load an uniform ion drift velocity V_{iy} with a value that satisfies the Harris equilibrium at the ambient thicker sheet that has $L = L_{\max} = 4d_i$ and $(T_i/T_e)_{\text{thick}} = 5$. This setup gets closer to an equilibrium in the limit of small V_{iy} that can be satisfied when the ambient thicker sheet is thick enough. A small drifting speed V_{iy} also reduces the drift-kink instability arising from ion shear flows between the ambient and sheet regions (Karimabadi et al., 2003). One may expect that particles would just stream out of the thin current sheet region, making the setup fall apart. However, it is not this case since the primary current carrier drift is the diamagnetic drift, where the guiding centers do not move.

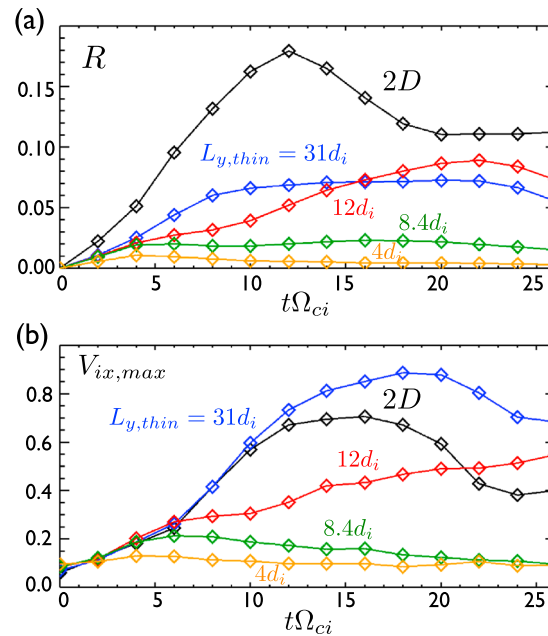


Figure 2. The time evolution of the normalized reconnection rate R and the maximum ion outflow speed $V_{ix,max}$ with different confinement scale $L_{y,thin}$.

3. Scaling of Reconnection Rates and Outflow Speeds

With this simulation setup, we can explore how reconnection rates and reconnection outflow speeds are affected by the confinement in the current direction. The results with $L_{y,thin} = 31d_i, 12d_i, 8.4d_i,$ and $4d_i$ are shown in Figure 2. For comparison, the results of the companion 2-D case is also plotted in black. This 2-D case employs the initial condition at the $y = 0$ plane of the 3-D simulations, which is basically the Harris sheet with a half thickness L_{min} . Given the symmetry of the system in the inflow direction, we can measure the reconnection rate using the increasing rate of the reconnected flux at the $z = 0$ plane; the total reconnected flux is $\Psi = \int_0^{L_x/2} \int_{-L_y/2}^{L_y/2} B_z(z=0) dx dy$, then the increasing rate of the reconnected flux is $d\Psi/dt$. To compare with 2-D, we define the reconnection rate as $R \equiv (d\Psi/dt)/L_{y,thin}$. For the $L_{y,thin} = 31d_i$ and $12d_i$ cases, both the reconnection rate and the maximum outflow speed are comparable to that in 2-D, where the X-line extent is infinitely long. For the $L_{y,thin} = 8.4d_i$ and $4d_i$ cases, we observe the significant impact from the reconnection region confinement, where both the rate and outflow speed plunge into much lower values. These suggest that the critical confinement scale that suppresses reconnection is $\lesssim 10d_i$. In the following, we look into the details of how reconnection works in two cases. The $L_{y,thin} = 31d_i$ case has realized 2-D-like fast reconnection in part of the thin current sheet, while the $L_{y,thin} = 8.4d_i$ case shows reconnection being strongly suppressed.

4. $L_{y,thin} = 31d_i$ Case

We show the evolution of the total current density $|J|$ of the $L_{y,thin} = 31d_i$ case at the $x = 0$ plane (right through the X-line) in Figure 3. The corresponding times are $0/\Omega_{ci}, 6/\Omega_{ci}, 12/\Omega_{ci},$ and $18/\Omega_{ci}$. The pair of white curves traces the location of $J_y \approx 0.15en_0V_A$, which is slightly larger than the background noise level, and they mark the boundary of the current sheet. Note that for z - y slice plots throughout this manuscript, ions are drifting upwardly (in the positive y direction), while electrons are drifting downwardly (in the negative y direction). We use the same color range for all plots of $|J|$ to facilitate the comparison of the current sheet thinning process. The current sheet thins asymmetrically and leads to a thinner sheet on the electron-drifting side. The bulge at time $18/\Omega_{ci}$ is caused by the generation of a secondary tearing mode, which will be discussed later in Figure 7.

In Figure 4, we look into the 3-D structure of the reconnection region at time $12/\Omega_{ci}$, after the reconnection rate reaching its maximum (i.e., check Figure 2). For reference, the current density at the $x = 0$ plane is shown again in Figure 4a. The reconnected field B_z at the $z = 0$ plane is shown Figure 4b, and

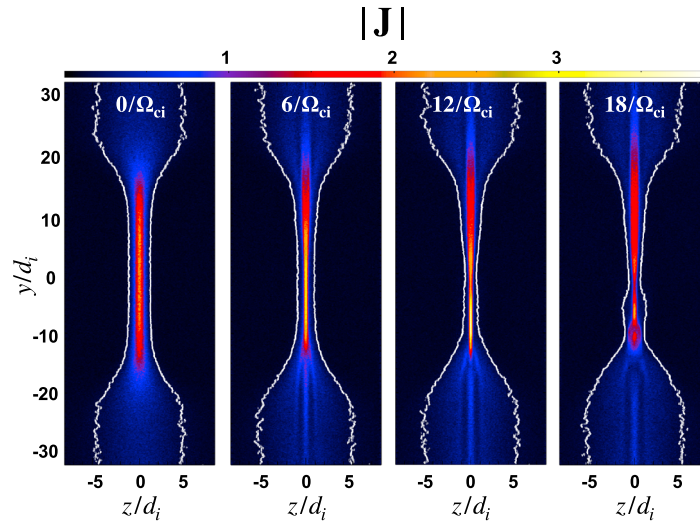


Figure 3. The evolution of the current density $|\mathbf{J}|$ on the $x = 0$ plane inside the 3-D box with $L_{y,\text{thin}} = 31d_i$. The white curves trace the boundary of the current sheet.

the ion outflow speed V_{ix} is shown in Figure 4c. Black regions cover the region of zero value, contrast the reconnecting region of colors. The X-line extent is revealed between the region of opposite B_z polarity near $x = 0$, and the true extent can still be approximated by $L_{y,\text{thin}} = 31d_i$. One pronounced feature is the asymmetric distribution of reconnection signatures in the y direction. The B_z signature is clearly shifted to the electron-drifting side. Inside this d_i -scale thin current sheet, it consists of two regions: One is the active region on the electron-drifting side with strong B_z and V_{ix} signatures. Another region on the ion-drifting side has weaker B_z and V_{ix} , indicating a suppressed reconnecting region; we refer it as the “suppression region” for short and we mark it with transparent white (or yellow) bands (i.e., as will be discussed in Figure 8b, this suppression region is best characterized by the significant decrease of the nonideal electric field strength from the fast rate value $\approx 0.1B_0V_A/c$ in the active region). Note that the extent of this suppression region is around $\approx 10d_i$. In Figure 4d, we make a x - z slice of the current density $|\mathbf{J}|$ at the active region (along the lower horizontal white dashed line indicated in Figure 4a). The morphology of the reconnection region is similar to that of a corresponding 2-D simulation (not shown). For comparison, in Figure 4e we make a similar slice at the suppression region (along the upper white horizontal dashed line indicated in Figure 4a). The current sheet near the X-line is thicker in comparison to that of the active region in Figure 4d.

Here we would like to point out that this two-region scenario is similar to that observed in two-fluid simulations (Meyer, 2015). However, the suppression region in particle-in-cell simulations has a localized X-line geometry on the x - z plane, while the suppression region in two-fluid model is more like a Sweet-Parker reconnection that has a long extended current sheet. The difference between two-fluid and kinetic descriptions of this region is interesting, indicating that the nature of the dissipation process plays a significant role in the results.

5. $L_{y,\text{thin}} = 8.4d_i$ Case

Here we show what happened if the extent of the thin current sheet is comparable or smaller than the extent of this suppressed reconnecting region discovered in the previous section. As already shown in Figure 2, both the reconnection rate and outflow speed drop significantly when $L_{y,\text{thin}} \lesssim 10d_i$, suggesting a switch-off of reconnection. Here we look into the details of the current sheet structure of the $L_{y,\text{thin}} = 8.4d_i$ case and describe the general property of having $L_{y,\text{thin}} \lesssim 10d_i$.

The evolution of the total current density $|\mathbf{J}|$ of the $L_{y,\text{thin}} = 8.4d_i$ case at the $x = 0$ plane (right through the X-line) is shown in Figure 5. The corresponding times are $0/\Omega_{ci}$, $6/\Omega_{ci}$, $12/\Omega_{ci}$, and $18/\Omega_{ci}$, the same as that discussed for the $L_{y,\text{thin}} = 31d_i$ case. The asymmetric thinning of the current sheet along the X-line is still recognizable, but the thinnest sheet on the electron-drifting side is not as thin as that at the active region of the $L_{y,\text{thin}} = 31d_i$ case shown in Figure 3. As a result, this case does not reach fast reconnection locally

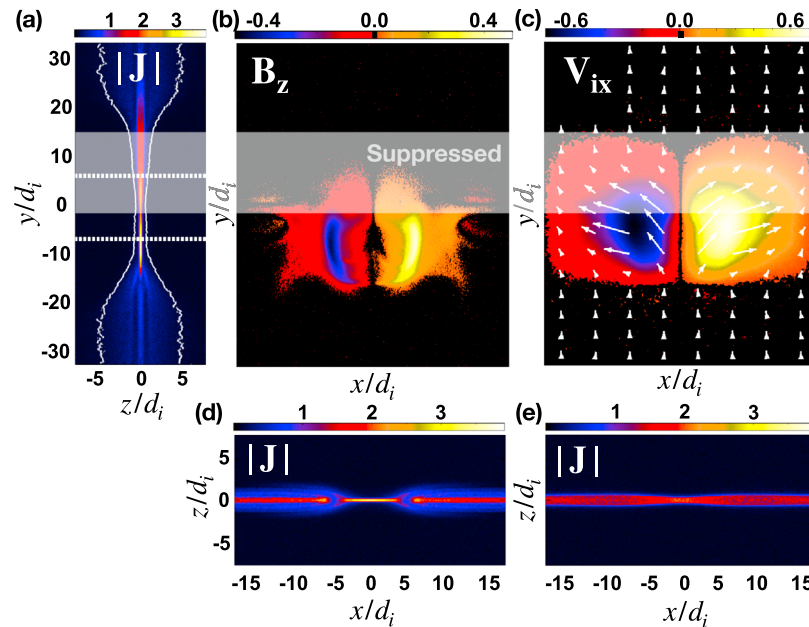


Figure 4. The 3-D structure of reconnection with $L_{y,\text{thin}} = 31d_i$ at time $12/\Omega_{ci}$. (a) The current density $|J|$ on the $x = 0$ plane. (b) The reconnected field B_z and (c) the ion outflow speed and the V_i vectors in white on the $z = 0$ plane. (d and e) The current density $|J|$ on the x - z plane along the lower and upper dashed lines in (a), respectively.

on the electron-drifting side and reconnection is strongly suppressed. We will discuss how this asymmetric thinning connects to the reconnection process in the next section.

The format in Figure 6 is the same as that in Figure 4. The ion outflow speed V_{ix} (in Figure 6c) is reduced by ≈ 6 times compared to that in Figure 4. It becomes clear that both the reconnected field B_z (in Figure 6b) and the outflow speed V_{ix} become narrower in y and concentrate on the electron-drifting side when $L_{y,\text{thin}}$ is smaller. Surprisingly, by comparing with Figure 6a, we realize that part of these more intense signatures are within the thick current sheet region. The real X-line extent manifested by the finite B_z on the x - y plane can still be approximated as $L_{y,\text{thin}} = 8.4d_i$. Figure 6d shows the current sheet structure on the slice along the lower horizontal line in Figure 6a, which passes through the strong B_z and V_{ix} regions. The current sheet is much thicker and the current density is reduced near $(x, z) = (0, 0)$. As will be discussed in the next section, the reconnected field B_z is swept into the thick current sheet but the magnetic tension $(\mathbf{B} \cdot \nabla)\mathbf{B}/4\pi \approx B_z \partial_z B_x/4\pi$ associated with the reconnected field lines remains active in driving outflows, although with a reduced speed.

6. The Extent of the Suppressed Reconnecting Region

The comparison of these two cases suggests the importance of the scale of this suppressed reconnecting region that fully develops within a long $L_{y,\text{thin}}$ current sheet. When $L_{y,\text{thin}} < L_{y,\text{suppression}} \approx O(10d_i)$, it appears that the current sheet can not thin toward the thickness required for fast reconnection, and thus, reconnection is strongly suppressed. The extent of this suppression region persists to have a similar y extent at later time as indicated in the structure of the reconnected magnetic field B_z in Figure 7. Also note that, at a later time $t = 18/\Omega_{ci}$, a secondary tearing mode is generated on the electron-drifting side, which further maps out the thinnest region of the entire X-line. An important question is then how to determine the spatial scale of this suppression region.

6.1. Three-Dimensional Ohm's Law

To achieve fast reconnection in collisionless plasmas, the d_i scale thin current sheet needs to thin further toward electron scale so that the frozen-in condition between electrons and magnetic fields can be broken. We quantify this effect using the generalized Ohm's law, which is basically the electron momentum

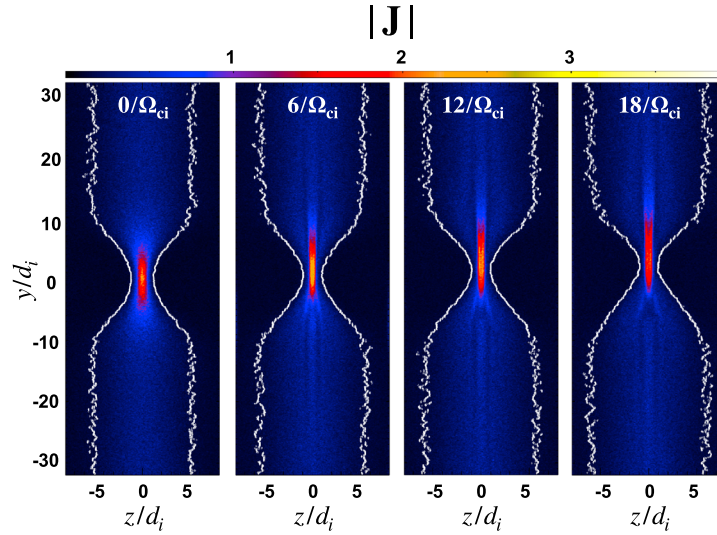


Figure 5. The evolution of the current density $|J|$ on the $x = 0$ plane inside the 3-D box with $L_{y,\text{thin}} = 8.4d_i$. The white curves trace the boundary of the current sheet.

equation:

$$\mathbf{E} + \frac{\mathbf{V}_e \times \mathbf{B}}{c} = -\frac{\nabla \cdot \mathbf{P}_e}{en_e} - \frac{m_e}{e} \mathbf{V}_e \cdot \nabla \mathbf{V}_e - \frac{m_e}{e} \partial_t \mathbf{V}_e. \quad (1)$$

The left-hand side measures the nonideal electric field that is supported by the nonideal terms on the right-hand side. The y component of the nonideal electric field is relevant to the reconnection electric field and its structure at the $x = 0$ plane is shown in Figure 8a. Within the active region between $y \in [-12, -2]d_i$, the magnitude of the nonideal electric field $E_y + (\mathbf{V}_e \times \mathbf{B})_y/c$ is $\simeq 0.12B_x V_{Ax}$, consistent with the typical value of the fast reconnection rate (Cassak et al., 2017; Liu et al., 2017). The contributions of the nonideal terms along the X-line are plotted in Figure 8b. Note that the “total” in black color sums up all terms and is negligible, indicating the excellent accuracy of this calculation. The $\partial_t V_{ey}$ term in orange color is also negligible, indicating a rather quasi steady state. Consistent with the standard 2-D simulation, the nonideal electric field in the active region is supported by the divergence of the pressure tensor $\nabla \cdot \mathbf{P}_e$ of which the primary contribution comes from the off-diagonal component, $\partial_x P_{exy} + \partial_z P_{ezy}$. To filter out a potential contribution from an electrostatic component (instead of the electromagnetic component) that does not contribute to reconnection, we apply the general magnetic reconnection theory (Hesse & Schindler, 1988; Schindler et al., 1988) to calculate the global 3-D reconnection rate. To evaluate the global rate, it requires to integrate E_{\parallel} along the magnetic field line that thread the ideal region to the localized nonideal region, then back to the ideal region on the other side. Since we do not expect a significant difference if an infinitesimal guide field is applied, we will integrate E_y along the X-line and note that $\int_0^{L_y} dy = \oint dy$ because of the periodic boundary condition in the y direction. The generation rate of the total reconnected flux is $\oint E_y dy = 2.1B_x V_{Ax} d_i$, and the corresponding 2-D rate is $(\oint E_y dy)/L_{y,\text{thin}} \simeq 2.1/31 = 0.068$, showing an excellent agreement with the value measured using $(\int B_z dx dy)/L_{y,\text{thin}}$ in Figure 2a.

In contrast to a 2-D model, now the ∂_y terms survive in the 3-D system. One of the new terms is $\partial_y P_{ey}$ in $\nabla \cdot \mathbf{P}_e$, another is the electron inertia term $\mathbf{V}_e \cdot \nabla \mathbf{V}_e = V_{ey} \partial_y V_{ey}$; note that both V_{ex} and V_{ez} vanish along the X-line due to the symmetry that coincides the flow stagnation point with the X-line. The closed integration $\oint V_{ey} \partial_y V_{ey} dy = \oint (1/2) \partial_y V_{ey}^2 dy = 0$ and here $\oint (1/en_e) \partial_y P_{ey} dy \simeq -0.018B_x V_{Ax} d_i$ that is 2 orders smaller compared to the contribution from the off-diagonal contribution $\oint (1/en_e) (\partial_x P_{exy} + \partial_z P_{ezy}) dy$. These two terms thus do not contribute to the integral $\oint E_y dy$ in this 3-D system, but they may redistribute E_y . The term $\partial_y P_{ey}$ contributes negatively to the nonideal electric field on the ion-drifting side, positively on the electron-drifting side. One may argue that, perhaps, $\partial_y P_{ey}$ on the ion-drifting side suppresses the typical fast reconnection electric field of order $0.1B_x V_{Ax}$ (Cassak et al., 2017; Liu et al., 2017). Thus, balancing $0.1B_x V_{Ax} \simeq (1/en_e) \partial_y P_{ey} \simeq (1/en_e) (B_x^2/8\pi)/L_{y,\text{suppression}}$ could lead to a gradient scale $L_{y,\text{suppression}}$ of an order $10d_i$ for the suppression region (i.e., in the last step, one may argue that the pressure difference is $\Delta P \simeq B_x^2/8\pi$).

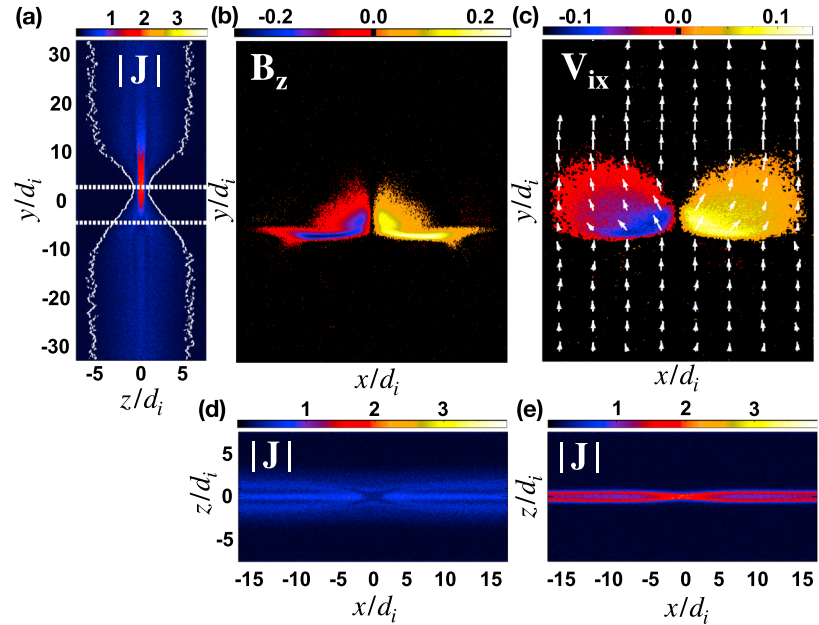


Figure 6. The 3-D structure of reconnection with $L_{y,\text{thin}} = 8.4d_i$ at time $18/\Omega_{ci}$. (a) The current density $|J|$ on the $x = 0$ plane. (b) The reconnected field B_z and (c) the ion outflow speed and the V_i vectors in white on the $z = 0$ plane. (d and e) The current density $|J|$ on the x - z plane along the lower and upper dashed lines in (a), respectively.

However, the $\partial_y P_{eyy}$ term shown here as the pink curve of Figure 8b is too small (compared to 0.1) to validate this argument. The electron inertia term $V_{ey}\partial_y V_{ey}$ contributes positively to the nonideal electric field on the ion-drifting side, negatively on the electron-drifting side. Similarly, one may construct an argument to infer the gradient scale of this term by balancing it with the fast reconnection rate, but its magnitude as shown by the blue curve of Figure 8b is also too small to be a valid explanation.

6.2. Time Scale Toward Fast Reconnection and Electron Drifts

In 2-D steady symmetric reconnection, the only nonideal term that can break the frozen-in condition right at the X-line is the divergence of the off-diagonal component of the pressure tensor, $\partial_x P_{exy} + \partial_z P_{ezy}$. For this term to be significant, it requires the current sheet to be thin enough and comparable to the electron gyroradius scale (ρ_e) so that the nongyrotopic feature develops (Hesse et al., 2011). (Here $\rho_e \approx 0.61d_e = 0.07d_i$ based on the initial electron pressure at the thin sheet and the reconnecting field.) Thus, to reach fast reconnection, the current sheet thinning is an unavoidable route. The tension force $B_z\partial_z B_x/4\pi$ rising from the reconnected magnetic flux B_z is required to drive outflow, which leads to current sheet thinning. In a 3-D system, we have an additional transport of this normal flux (B_z) in the electron drift direction below the d_i scale, because ions are demagnetized while electrons are still magnetized (i.e., the Hall effect). This transport removes this flux from what becomes the suppressed part of the reconnecting X-line. This removal of B_z prevents outflows and, hence, thinning of the current sheet. As a consequence, the current sheet thickness in the $L_{y,\text{thin}} = 8.4d_i$ case cannot reach the thinnest thickness as that in the $L_{y,\text{thin}} = 31d_i$ case, and this appears to throttle reconnection.

The electron drift speed along the anticurrent ($-y$) direction consists of the $\mathbf{E} \times \mathbf{B}$ drift and the diamagnetic drift, $\mathbf{V}_{e,\perp} \approx c(\mathbf{E} \times \mathbf{B})_y/B^2 - c(\mathbf{B} \times \nabla \cdot \mathbf{P})_y/en_e B^2$. The primary components are

$$V_{ey} \approx c \frac{E_z B_x}{B^2} + \frac{c B_x \partial_z P_{ezz}}{en_e B^2}. \quad (2)$$

The diamagnetic drift (\mathbf{V}^* in green) dominates the electron drift within this thin current sheet, as shown in Figure 8c. Note that a diamagnetic drift can also transport the magnetic flux even though the guiding centers of electrons do not really move (i.e., roughly speaking, we can swap x and y and assume $B_z \ll B_x$ in equation (2) here to recover equation (1) of Liu & Hesse, 2016, that transports the reconnected flux as indicated in equation (2) therein. See also Coppi, 1965; Swisdak et al., 2003). This preferential flux transportation by electrons results in the enhanced reconnected magnetic flux B_z on the electron-drifting sides

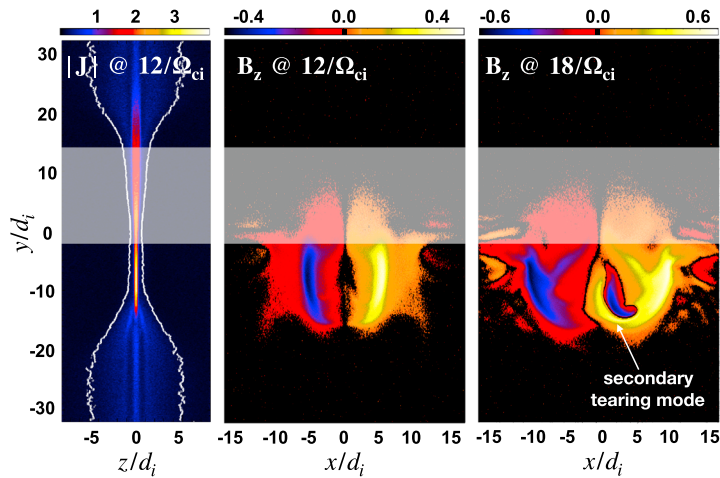


Figure 7. The structure of the reconnected magnetic field B_z on the $z = 0$ plane at later time in the $L_{y,\text{thin}} = 31d_i$ case.

shown in Figures 4b and 6b. This transport also explains why the current sheet only becomes thinner on the electron-drifting side as shown in Figures 3 and 5 and the preferential occurrence of the secondary tearing mode on the electron-drifting side as shown in Figure 7.

One can then imagine that the time scale of the current sheet thinning process toward fast reconnection can be translated into the spatial scale of the suppressed reconnecting region, and it is

$$L_{y,\text{suppression}} \simeq T_{\text{thinning}} \times V_{ey}. \quad (3)$$

The electron drift speed is of the order of V_{Ax} inside this suppression region. On the other hand, reconnection in the $L_{y,\text{thin}} = 31d_i$ case reaches the maximum rate at time $\simeq 10/\Omega_{ci}$ as shown by the blue curve in Figure 2a; thus, $T_{\text{thinning}} \simeq 10/\Omega_{ci}$. (Note that this time scale in 3-D is comparable to the time scale of the companion 2-D simulation shown in black color.) The rough estimation of equation (3) suggests that the extent of this suppression region should be of the order of $L_{y,\text{suppression}} \simeq 10/\Omega_{ci} \times V_{Ax} = 10d_i$, which agrees with the observed spatial scale. More accurately, we can integrate the time for the flux to be transported within the suppression region (marked by the yellow band that spans $y \in [-2, 14]d_i$) using the V_{ey} profile in Figure 8c. It estimates the transport time scale $T_{\text{transport}} = \int (dy/V_{ey}) \simeq 10/\Omega_{ci}$ that compares favorably to the thinning

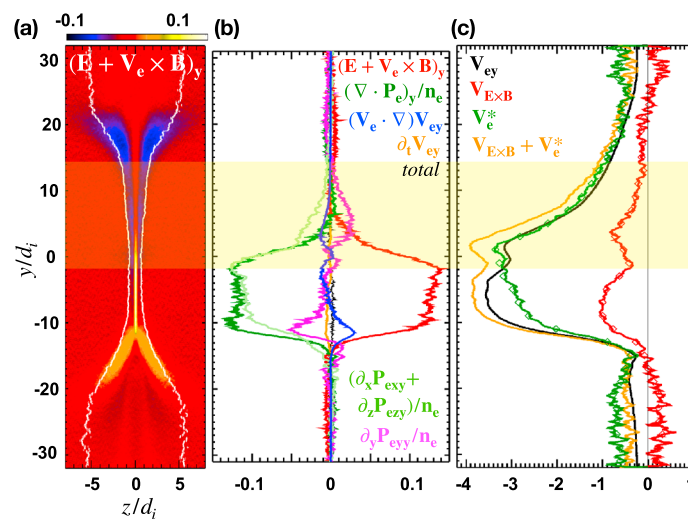


Figure 8. Analyses of the $L_{y,\text{thin}} = 31d_i$ case at time $12/\omega_{ci}$. (a) The nonideal electric field $(\mathbf{E} + \mathbf{V}_e \times \mathbf{B})_y$ on the $x = 0$ plane. (b) The decomposition of the nonideal electric field along the $(x, z) = (0, 0)$ line. (c) The decomposition of the electron drift near the X-line.

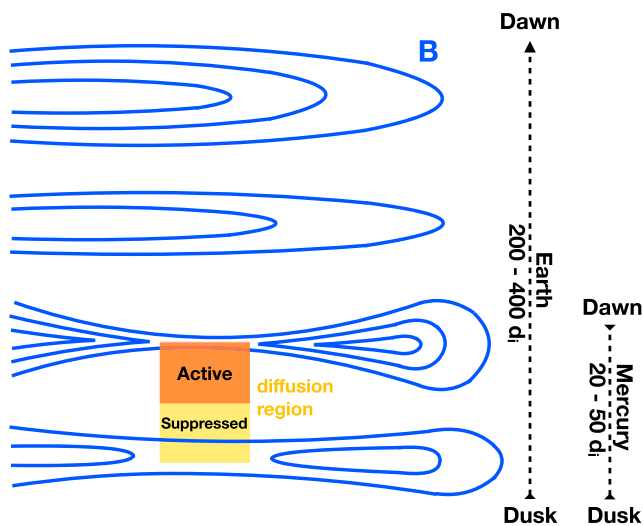


Figure 9. An explanation of why the dawn-dusk asymmetry is opposite at Earth and Mercury based on the dawn-ward transport of normal magnetic fields (B_z) and reconnection physics. (Note that in this figure the dawnside and duskside are switched vertically to follow the convention.)

time scale T_{thinning} just discussed. This quantitative examination validates this flux-transport mechanism in determining the extent of the suppression region.

7. Summary and Discussion on the Dawn-Dusk Asymmetry

We modified the Harris sheet geometry to embed an inertial scale (d_i) thin current sheet between much thicker sheets in the current direction. The resulting reconnection is well confined within the thin current sheet. With this machinery, we investigate the shortest possible X-line extent for fast reconnection, which appears to be $\approx 10d_i$. The time scale for a d_i -scale current sheet to thin toward the condition suitable for fast reconnection (with a normalized reconnection rate ≈ 0.1) can be translated into an intrinsic length scale $\approx 10d_i$ of a suppressed reconnecting region after considering the flux transport along the X-line (equation (3)), because the reconnected magnetic flux (B_z) required to drive outflows and further the current sheet thinning is transported away in the anticurrent direction by electrons below the ion inertial scale (i.e., the Hall effect). We do not expect a strong dependence of this critical length on the mass ratio. The nonlinear growth time of reconnection appears to be virtually independent on mass ratio, and so does the flux transport; this is consistent with the apparent independence of the reconnection rate on the mass ratio

(Hesse et al., 1999; Shay & Drake, 1998). Simulations demonstrate that reconnection is strongly suppressed if the extent of the thin current sheet is shorter than this intrinsic length scale of the suppressed reconnecting region. In these short $L_{y,\text{thin}}$ cases, the outflow driver B_z is completely removed from the reconnecting region. The current sheet thus is not able to thin to the thickness where the nongyrotropic feature of the electron pressure tensor develops and becomes significant for breaking the frozen-in condition at the X-line.

Reconnection is strongly suppressed when the X-line extent is shorter than the length scale of the suppressed reconnecting region $L_{y,\text{suppression}} \approx O(10d_i)$, and this may explain the narrowest possible DFB observed at Earth's magnetotail (Liu et al., 2015). Note that an interchange/ballooning instability may locally trigger reconnection (e.g., Pritchett, 2013) and our basic conclusion on the minimal X-line extent should still hold in the complex coupling to an instability. On the other hand, this internal dawn-dusk asymmetry of the reconnection X-line (e.g., Figure 7) may also explain why the flux transport events occur preferentially on the dawnside of Mercury's magnetotail (Sun et al., 2016). The fact that the active region preferentially occurs on the electron-drifting side (i.e., the dawnside) seems to contradict to the explanation of the dawn-dusk asymmetry discussed in Lu et al. (2016, 2018). Here we clarify the similarity and difference of our studies, which leads to a plausible explanation to the opposite dawn-dusk asymmetry observed at Earth (Nagai et al., 2013; Runov et al., 2017; Slavin et al., 2005) and Mercury (Sun et al., 2016). While the electron drift transports the normal magnetic flux (B_z) in both studies, the important difference stems from the role of the normal magnetic field (B_z) discussed. In Lu et al. (2016, 2018), the initial normal magnetic field B_z associated with the tail geometry inhibits the onset of reconnection since it prevents the current sheet from being tearing unstable (Hesse & Schindler, 2001; Liu et al., 2014; Sitnov & Schindler, 2010). Reconnection onsets are thus easier on the duskside since these B_z flux is transported to the dawnside. In contrast, the reconnected field (B_z) discussed here drives outflows and furthers the thinning toward fast reconnection after reconnection onset. As illustrated using Figure 9, the explanation of the dawn-dusk asymmetry in Lu et al. (2016, 2018) can remain valid in predicting the global asymmetry of reconnection “onset locations” on the duskside of Earth. While our study explains the “internal” asymmetric structure of the X-line within these onset locations, that gives rise to the active region on the dawnside locally.

For Mercury, if one considered a proton density of $\sim 3 \text{ cm}^{-3}$ (Gershman et al., 2014; Poh et al., 2018; Sun et al., 2018), and the relatively thin current sheet width in Mercury's tail near midnight is $\sim 2R_M$ where $1R_M \sim 2,440 \text{ km}$ (Poh et al., 2017; Rong et al., 2018; Sun et al., 2016), then the global dawn-dusk extent is $\sim 37d_i$, comparable to our $31d_i$ case studied here. While for Earth, the proton density in the plasma sheet is around an order of magnitude smaller than that at Mercury (Baumjohann et al., 1989; Huang & Frank,

1994; Sun et al., 2018), and the width of the relatively thin current sheet near midnight is $\sim 20 R_E$ (Nakai et al., 1991; Zhang et al., 2016), corresponding to $\sim 300 d_i$. The dawn-dusk extent of the thin current sheet region at the magnetotail of Mercury is thus much shorter (in terms of d_i) than that of Earth. Therefore, the entire magnetotail of Mercury likely only manifests the internal dawn-dusk asymmetry of the X-line with the active region and secondary tearing modes appearing on the dawnside, as emphasized by the orange region of Figure 9. We further predict that magnetic reconnection may not occur in a planetary magnetotail if its global dawn-dusk extent is $\ll 10 d_i$. Finally, while these arguments are purely based on the reconnection physics in the plasma sheet, we acknowledge that global effects (e.g., Keesee et al., 2011; Lotko et al., 2015; Spence & Kivelson, 1993; Walsh et al., 2014) could also be important but are beyond the scope of this study.

Acknowledgments

Y.-H. Liu thanks M. Swisdak, S. Lu, S. Wang, A. M. Keesee, and M. Shay for helpful discussions. Y. H. L. and T. C. L. were supported by NASA grant 80NSSC18K0754 and MMS mission. M. H. was supported by the Research Council of Norway/CoE under contract 223252/F50 and by NASA's MMS mission. J. L. was supported by NSF grant 1401822 and NASA contract NAS5-02099. J. A. S. was supported by NASA MMS GI grant 80NSSC18K1363. Simulations were performed with NERSC Advanced Supercomputing, LANL institutional computing, and NASA Advanced Supercomputing. The data sets and scripts used to make the plots of this paper can be found at the Zenodo (<https://doi.org/10.5281/zenodo.2603141>).

References

- Angelopoulos, V., McFadden, J. P., Larson, D., Carlson, C. W., Mende, S. B., Frey, H., et al. (2008). Tail reconnection triggering substorm onset. *Science*, *321*, 931–935.
- Arnold, H., Swisdak, M., & Drake, J. F. (2018). Characterizing ion flows across a magnetotail dipolarization jet. *Journal of Geophysical Research: Space Physics*, *123*, 6326–6334. <https://doi.org/10.1029/2018JA025604>
- Baker, D. N., Pulkkinen, T. I., Angelopoulos, V., Baumjohann, W., & McPherron, R. L. (1996). Neutral line model of substorms: Past results and present view. *Journal of Geophysical Research*, *101*(12), 975.
- Baumjohann, W., Pashchmann, G., & Cattell, C. A. (1989). Average plasma properties in the central plasma sheet. *Journal of Geophysical Research*, *94*, 6597.
- Birn, J., Liu, Y.-H., Daughton, W., Hesse, M., & Schindler, K. (2015). Reconnection and interchange instability in the near magnetotail. *Earth, Planets and Space*, *67*, 110.
- Birn, J., Nakamura, R., Panov, E. V., & Hesse, M. (2011). Bursty bulk flows and dipolarization in MHD simulations of magnetotail reconnection. *Journal of Geophysical Research*, *116*, A01210. <https://doi.org/10.1029/2010JA016083>
- Cassak, P. A., Liu, Yi-Hsin, & Shay, M. A. (2017). A review of the 0.1 reconnection rate problem. *Journal of Plasma Physics*, *83*, 715830501.
- Coppi, B. (1965). Current driven instabilities in configurations with sheared magnetic fields. *Physics of Fluids*, *8*, 2273.
- Daughton, W. (1999). The unstable eigenmodes of a neutral sheet. *Physics of Plasmas*, *6*, 1329.
- Dorfman, S., Ji, H., Yamada, M., Lawrence, E., Myers, C., & Tharp, T. D. (2014). Experimental observation of 3-D, impulsive reconnection events in a laboratory plasma. *Physics of Plasmas*, *21*, 012109.
- Gershman, D. J., Slavin, J. A., Raines, J. M., Zurbuchen, T. H., Anderson, B. J., Korth, H., et al. (2014). Ion kinetic properties in Mercury's pre-midnight plasma sheet. *Geophysical Research Letters*, *41*, 5740. <https://doi.org/10.1002/2014GL060468>
- Harris, E. G. (1962). On a plasma sheath separating regions of one directional magnetic field. *Nuovo Cimento*, *23*, 115.
- Hesse, M., Neukirch, T., Schindler, K., Kuznetsova, M., & Zenitani, S. (2011). The diffusion region in collisionless magnetic reconnection. *Space Science Reviews*, *160*, 3–23.
- Hesse, M., & Schindler, K. (1988). A theoretical foundation of general magnetic reconnection. *Journal of Geophysical Research*, *93*(A6), 5559–5567.
- Hesse, M., & Schindler, K. (2001). The onset of magnetic reconnection in the magnetotail. *Earth, Planets and Space*, *53*, 645–653.
- Hesse, M., Schindler, K., Birn, J., & Kuznetsova, M. (1999). The diffusion region in collisionless magnetic reconnection. *Physics of Plasmas*, *6*, 1781–1795.
- Huang, C. Y., & Frank, L. A. (1994). A statistical survey of the central plasma sheet. *Journal of Geophysical Research*, *99*, 83.
- Karimabadi, H., Daughton, W., Pritchett, P. L., & Krauss-Varban, D. (2003). Ion-ion kink instability in the magnetotail: 1. Linear theory. *Journal of Geophysical Research*, *108*(A11), 1400. <https://doi.org/10.1029/2003JA010026>
- Keesee, A. M., Buzulukova, N., Goldstein, J., McComas, D. J., Scime, E. E., Spence, H., et al. (2011). Remote observations of ion temperatures in the quiet time magnetosphere. *Geophysical Research Letters*, *38*, L03104. <https://doi.org/10.1029/2010GL045987>
- Kepko, L., McPherron, R. L., Amm, O., Apatenkov, S., Baumjohann, W., Birn, J., et al. (2015). Substorm current wedge revisited. *Space Science Reviews*, *190*, 1.
- Kronberg, E. A., Woch, J., Krupp, N., Lagg, A., Khurana, K. K., & Glassmeier, K.-H. (2005). Mass release at Jupiter: Substorm-like processes in the Jovian magnetotail. *Journal of Geophysical Research*, *110*, A03211. <https://doi.org/10.1029/2004JA010777>
- Lapenta, G., & Bettarini, L. (2011). Self-consistent seeding of the interchange instability in dipolarization fronts. *Geophysical Research Letters*, *38*, L11102. <https://doi.org/10.1029/2011GL047742>
- Li, S.-S., Angelopoulos, V., Runov, A., & Kiehas, S. A. (2014). Azimuthal extent and properties of midtail plasmoids from two-point ARTEMIS observations at the Earth-Moon Lagrange points. *Journal of Geophysical Research: Space Physics*, *119*, 1781–1796. <https://doi.org/10.1002/2013JA019292>
- Li, T. C., Yi-Hsin Liu, M. H., & Zou, Y. (2019). 3D x-line spreading in asymmetric magnetic reconnection. in preparation.
- Liu, J., Angelopoulos, V., Zhou, X.-Z., Runov, A., & Yao, Z. (2013). On the role of pressure and flow perturbations around dipolarizing flux bundles. *Journal of Geophysical Research: Space Physics*, *118*, 7104–7118. <https://doi.org/10.1002/2013JA019256>
- Liu, J., Angelopoulos, V., Zhou, X.-Z., Yao, Z.-H., & Runov, A. (2015). Cross-tail expansion of dipolarizing flux bundles. *Journal of Geophysical Research: Space Physics*, *120*, 2516–2530. <https://doi.org/10.1002/2015JA020997>
- Liu, Y.-H., Birn, J., Daughton, W., Hesse, M., & Schindler, K. (2014). Onset of reconnection in the near magnetotail: PIC simulations. *Journal of Geophysical Research: Space Physics*, *119*, 9773–9789. <https://doi.org/10.1002/2014JA020492>
- Liu, Y.-H., & Hesse, M. (2016). Suppression of collisionless magnetic reconnection in asymmetric current sheets. *Physics of Plasmas*, *23*, 060704.
- Liu, Y.-H., Hesse, M., Guo, F., Daughton, W., Li, H., Cassak, P. A., & Shay, M. A. (2017). Why does steady-state magnetic reconnection have a maximum local rate of order 0.1? *Physical Review Letters*, *118*, 085101.
- Lotko, W., Smith, R. H., Zhang, B., Quellet, J. E., Brambles, O. J., & Lyon, J. G. (2015). Ionospheric control of magnetotail reconnection. *Science*, *345*, 184.
- Lu, S., Lin, Y., Angelopoulos, V., Artemyev, A. V., Pritchett, P. L., Lu, Q., & Wang, X. Y. (2016). Hall effect control of magnetotail dawn-dusk asymmetry: A three-dimensional global hybrid simulation. *Journal of Geophysical Research: Space Physics*, *121*, 11,882–11,895. <https://doi.org/10.1002/2016JA023325>

- Lu, S., Pritchett, P. L., Angelopoulos, V., & Artemyev, A. V. (2018). Formation of dawn-dusk asymmetry in Earth's magnetotail thin current sheet: A three-dimensional particle-in-cell simulation. *Journal of Geophysical Research: Space Physics*, *123*, 2801–2814. <https://doi.org/10.1002/2017JA025095>
- Meyer, J. C. (2015). Structure of the diffusion region in three dimensional magnetic reconnection (PhD thesis), University of Delaware.
- Mitchell, D. G., Brandt, P. C., Roelof, E. C., Dandouras, J., Krimigis, S. M., Mauk, B. H., et al. (2005). Energetic ion acceleration in Saturn's magnetotail: Substorm at Saturn? *Journal of Geophysical Research*, *32*, L20S01. <https://doi.org/10.1029/2005GL022647>
- Nagai, T., Shinohara, I., Zenitani, S., Nakamura, R., Nakamura, T. K. M., Fujimoto, M., et al. (2013). Three-dimensional structure of magnetic reconnection in the magnetotail from geotail observations. *Journal of Geophysical Research: Space Physics*, *118*, 1667–1678. <https://doi.org/10.1002/jgra.50247>
- Nakai, H., Kamide, Y., & Russell, C. T. (1991). Influence of solar wind parameters and geomagnetic activity on the tail lobe magnetic field: A statistical study. *Journal of Geophysical Research*, *96*, 5511–5523.
- Nakamura, R., Baumjohann, W., Mouikis, C., Kistler, L. M., Runov, A., Volwerk, M., et al. (2004). Spatial scale of high-speed flows in the plasma sheet observed by cluster. *Geophysical Research Letters*, *31*, L09804. <https://doi.org/10.1029/2004GL019558>
- Nakamura, T. K. M., Nakamura, R., Alexandrova, A., Kubota, Y., & Nagai, T. (2012). Hall magnetohydrodynamic effects for three-dimensional magnetic reconnection with finite width along the direction of the current. *Journal of Geophysical Research*, *117*, A03220. <https://doi.org/10.1029/2011JA017006>
- Poh, G., Slavin, J. A., Jia, X., Raines, J. M., Imber, S. M., Sun, W. J., et al. (2017). Coupling between Mercury and its nightside magnetosphere: Cross-tail current sheet asymmetry and substorm current wedge formation. *Journal of Geophysical Research: Space Physics*, *122*, 8419–8433. <https://doi.org/10.1002/2017JA024266>
- Poh, G., Slavin, J. A., Jia, X., Sun, W.-J., Raines, J. M., Imber, S. M., et al. (2018). Transport of mass and energy in Mercury's plasma sheet. *Geophysical Research Letters*, *45*, 12,163–12,170. <https://doi.org/10.1029/2018GL080601>
- Pritchett, P. L. (2013). The onset of magnetic reconnection in three dimensions. *Physics of Plasmas*, *20*, 080703.
- Pritchett, P., Coroniti, F. V., & Nishimura, Y. (2014). The kinetic ballooning/interchange instability as a source of dipolarization fronts and auroral streamers. *Journal of Geophysical Research: Space Physics*, *119*, 4723–4739. <https://doi.org/10.1002/2014JA019890>
- Pritchett, P., & Lu, S. (2018). Externally driven onset of localized magnetic reconnection and disruption in a magnetotail configuration. *Journal of Geophysical Research: Space Physics*, *123*, 2787–2800. <https://doi.org/10.1002/2017JA025094>
- Rong, Z. J., Ding, Y., Slavin, J. A., Zhong, J., Poh, G., Sun, W. J., et al. (2018). The magnetic field structure of Mercury's magnetotail. *Journal of Geophysical Research: Space Physics*, *123*, 548–566. <https://doi.org/10.1002/2017JA024923>
- Runov, A., Kiehas, S. A., & Li, S.-S. (2017). Dawn-dusk asymmetries in magnetotail transients. In S. Haaland, A. Runov, & C. Forsyth (Eds.), *Dawn-dusk asymmetries in planetary plasma environments*. Hoboken, NJ: John Wiley. <https://doi.org/10.1002/9781119216346.ch18>
- Schindler, K., Hesse, M., & Birn, J. (1988). General magnetic reconnection, parallel electric fields, and helicity. *Journal of Geophysical Research*, *93*(A6), 5547–5557.
- Shay, M. A., & Drake, J. F. (1998). The role of electron dissipation on the rate of collisionless magnetic reconnection. *Geophysical Research Letters*, *25*(20), 3759–3762.
- Shay, M. A., Drake, J. F., Swisdak, M., Dorland, W., & Rogers, B. N. (2003). Inherently three dimensional magnetic reconnection: A mechanism for bursty bulk flows? *Geophysical Research Letters*, *30*(6), 1345. <https://doi.org/10.1029/2002GL016267>
- Shepherd, L. S., & Cassak, P. A. (2012). Guide field dependence of 3-D X-line spreading during collisionless magnetic reconnection. *Journal of Geophysical Research*, *117*, A10101. <https://doi.org/10.1029/2012JA017867>
- Sitnov, M. I., Merkin, V. G., Swisdak, M., Motoba, T., Buzulukova, N., Moore, T. E., et al. (2014). Magnetic reconnection, buoyancy, and flapping motions in magnetotail explosions. *Journal of Geophysical Research: Space Physics*, *119*, 7151–7168. <https://doi.org/10.1002/2014JA020205>
- Sitnov, M. I., & Schindler, K. (2010). Tearing stability of a multiscale magnetotail current sheet. *Geophysical Research Letters*, *37*, L08102. <https://doi.org/10.1029/2010GL042961>
- Slavin, J. A., Anderson, B. J., Baker, D. N., Benna, M., Boardsen, S. A., Gloeckler, G., et al. (2010). MESSENGER observations of extreme loading and unloading of Mercury's magnetic tail. *Science*, *329*, 665.
- Slavin, J. A., Tanskanen, E. I., Hesse, M., Owen, C. J., Dunlop, M. W., Imber, S., et al. (2005). Cluster observations of traveling compression regions in the near-tail. *Journal of Geophysical Research*, *110*, A06207. <https://doi.org/10.1029/2004JA010878>
- Southwood, D. J., & Chané, E. (2016). High-latitude circulation in giant planet magnetosphere. *Journal of Geophysical Research: Space Physics*, *121*, 5394–5403. <https://doi.org/10.1002/2015JA022310>
- Spence, H. R., & Kivelson, M. G. (1993). Contributions of the low-latitude boundary layer to the finite width magnetotail convection model. *Journal of Geophysical Research*, *98*, 15,487–15,496.
- Sun, W. J., Fu, S. Y., Slavin, J. A., Raines, J. M., Zong, Q. G., Poh, G. K., & Zurbuchen, T. H. (2016). Spatial distribution of Mercury's flux ropes and reconnection fronts: MESSENGER observations. *Journal of Geophysical Research: Space Physics*, *121*, 7590–7607. <https://doi.org/10.1002/2016JA022787>
- Sun, W. J., Raines, J. M., Fu, S. Y., Slavin, J. A., Wei, Y., Poth, G. K., et al. (2017). MESSENGER observations of the energization and heating of protons in the near-Mercury magnetotail. *Geophysical Research Letters*, *44*, 8149–8158. <https://doi.org/10.1002/2017GL074276>
- Sun, W. J., Slavin, J. A., Dewey, R. M., Raines, J. M., Fu, S. Y., Wei, Y., et al. (2018). A comparative study of the proton properties of magnetospheric substorms at Earth and Mercury in the near magnetotail. *Geophysical Research Letters*, *45*, 7933–7941. <https://doi.org/10.1029/2018GL079181>
- Sun, W. J., Slavin, J. A., Fu, S. Y., Raines, J. M., Zong, Q.-G., Imber, S. M., et al. (2015). MESSENGER observations of magnetospheric substorm activity in Mercury's near magnetotail. *Geophysical Research Letters*, *42*, 3692–3699. <https://doi.org/10.1002/2015GL064052>
- Swisdak, M., Rogers, B. N., Drake, J. F., & Shay, M. A. (2003). Diamagnetic suppression of component magnetic reconnection at the magnetopause. *Journal of Geophysical Research*, *108*(A5), 1218. <https://doi.org/10.1029/2002JA009726>
- Walsh, A. P., Haaland, S., Forsyth, C., Keese, A. M., Kissinger, J., Li, K., et al. (2014). Dawn-dusk asymmetries in the coupled solar wind-magnetosphere-ionosphere system: A review. *Annales de Geophysique*, *32*, 705.
- Zhang, S., Tian, A., Shi, Q., Sun, W., Yao, Z., Fu, S., et al. (2016). A statistical study of the plasma sheet in the near and middle Earth magnetotail. *Chinese Journal of Geophysics*, *59*, 411.